Radboud Repository

Radboud University Nijmegen

PDF hosted at the Radboud Repository of the Radboud University Nijmegen

The following full text is a publisher's version.

For additional information about this publication click this link.
http://hdl.handle.net/2066/169105

Please be advised that this information was generated on 2019-09-17 and may be subject to change.

This is an open access article published under a Creative Commons Non-Commercial No Derivative Works (CC-BY-NC-ND) Attribution License, which permits copying and redistribution of the article, and creation of adaptations, all for non-commercial purposes.

ACSNANO www.acsnano.org

ARTICLE

Biodegradable Hybrid Stomatocyte Nanomotors for Drug Delivery

Yingfeng Tu,[†] Fei Peng,[†] Alain A. M. André,[†] Yongjun Men,[†] Mangala Srinivas,[‡] and Daniela A. Wilson*[,†]

[†]Institute for Molecules and Materials, Radboud University Nijmegen, Heyendaalseweg 135, 6525 AJ Nijmegen, The Netherlands

[‡]Radboud Institute for Molecular Life Sciences, Radboud University Medical Center, Geert Grooteplein 28, 6525 GA Nijmegen, The Netherlands

Supporting Information

ABSTRACT: **We report the self-assembly of a biodegradable platinum nanoparticle-loaded stomatocyte nanomotor containing both PEG-*b*-PCL and PEG-*b*-PS as a potential candidate for anticancer drug delivery. Well-defined stomatocyte structures could be formed even after incorporation of 50% PEG-*b*-PCL polymer. Demixing of the two polymers was expected at high percentage of semicrystalline poly(*ε*-caprolactone) (PCL), resulting in PCL domain formation onto the membrane due to different properties of two polymers. The biodegradable motor system was further shown to move directionally with speeds up to 39 *μ*m/s by converting chemical fuel, hydrogen peroxide, into mechanical motion as well as rapidly delivering the drug to the targeted cancer cell. Uptake by cancer cells and fast doxorubicin drug release was demonstrated during the degradation of the motor system. Such biodegradable nanomotors provide a convenient and efficient platform for the delivery and controlled release of therapeutic drugs.**

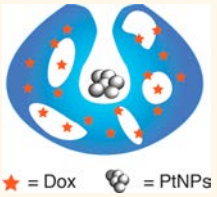

KEYWORDS: *nanomotors, drug delivery, biodegradable, self-assembly, hybrid*

Inspired by fascinating molecular motors and movable organisms, scientists have used both top-down and bottom-up strategies to fabricate self-propelled micro- and nanomotors over the past decade.[1−9] Until now, many examples of different types of motors (micro- and nanotubes,[10−12] wires,[13,14] helices,[15,16] rods,[17−19] Janus motors[20−23] and self-assembled polymeric motors[24−28]) have been developed. These artificial motors are capable of converting chemical or external energy into autonomous movement and possess various potential applications such as environmental remediation, sensing, and drug delivery.[29−34] Compared to normal drug delivery systems (lacking self-driving force), the most important advantage of a micro- and nanomotor system is independent impetus, which is necessary for tissue penetration and cellular barriers.[34,35] For drug delivery applications, micro- and nanomotor systems should be both biocompatible and biodegradable.[36,37] However, the design of current motor systems reported so far is mostly based on heavy metal systems, which do not provide a suitable soft interface for biological systems.[14,38]

While several examples of biocompatible motors have already been reported,[21,39,40] only a few that progress toward biodegradable motor systems have been reported until now.[41−45] For degradable zinc (Zn)/magnesium (Mg)-based micromotors, acid-powered propulsion can be achieved only in the gastrointestinal tract. The main degradation products were essential nutrients in human bodies.[46,47] A protein-based biodegradable multilayer microtubular motor combined with drug-loaded gelatin hydrogel has also been reported recently.[42] However, the size of the Zn/Mg or protein-based motor is micron sized, which is far away from potential clinical applications that target an intravenous route. Furthermore, the clearance of these micrometer motors will be quite fast due to the lack of poly(ethylene glycol) (PEG) shells. In general, the introduction of PEG shells, called PEGylation, onto the surface of micro- and nanocarriers can prolong their circulation *in vivo* by avoiding phagocytosis from macrophages.[48] Hence, the development of nanometer-scale biodegradable motors capable of stealth transport and drug release remains challenging.

In our previous work, a polymeric stomatocyte nanomotor made of soft self-assembled block copolymers based on poly(ethylene glycol)-*b*-polystyrene (PEG-*b*-PS) was demonstrated not only to move in the presence of hydrogen peroxide[49] and alternative fuels[50,51] but also to show chemotaxis behavior upon hydrogen peroxide gradients.[24] Unlike the traditional motor systems, both water-soluble and water-insoluble drugs can be loaded due to the presence of the bilayer structure.[52] However, as a major component, glassy PS is unfortunately a non-biodegradable and non-biocompatible polymer, which is not suitable for further biomedical applications. This fully bottom-up nanomotor system would

Received: December 2, 2016
Accepted: February 10, 2017
Published: February 10, 2017

 © 2017 American Chemical Society

DOI: 10.1021/acsnano.6b08079
ACS Nano 2017, 11, 1957−1963

be more versatile if a biodegradable polymer was used to build the structure of the stomatocyte.

Here, we demonstrate successful design and fabrication of a biodegradable self-assembled nanomotor system for drug delivery based on a mixture of poly(ethylene glycol)-*b*-poly(ε-caprolactone) (PEG-*b*-PCL) and well-documented vesicle former PEG-*b*-PS, as illustrated in Figure 1. Biodegradable polymer PCL is one of the most commonly used candidates and was already approved by the FDA for medical applications.[53,54] Stomatocyte bowl-shape morphology was obtained under osmotic folding of polymersomes and was observed even when the percentage of PEG-*b*-PCL was increased to 50% (w/w, 67% in mol ratio). The hydrophilic polymer PEG in our system can prolong the circulation time *in vivo*. Furthermore, water-soluble anticancer drug doxorubicin (DOX) was loaded into the lumen of the structure, and platinum nanoparticles (PtNPs, as model catalyst) were encapsulated in the cavity of stomatocyte as the engine. The self-assembled nanomotors show autonomous motion under low concentrations of hydrogen peroxide. Due to the different structural properties of PCL, which is a semicrystalline polymer, and PS, a glassy polymer, it was anticipated that upon mixing the PCL would demix and form domains in the self-assembled bilayer when a high percentage of PCL was blended into the membrane of stomatocytes. Large pores would be formed onto the stomatocyte surface during the degradation of PCL, which could lead to sustained drug release. After uptake by tumor cells, the biodegradable stomatocyte nanomotor could subsequently release the loaded cargo, in this case, Dox in tumor cells (HeLa cells). According to the literature, tumor cells can produce hydrogen peroxide at a rate of up to 0.5 nmol per 10^4 cells per hour.[55] Therefore, such a design enables our drug-loaded nanomotor system to actively move toward tumor cells, facilitate uptake, release the drug, and kill the tumor cells.

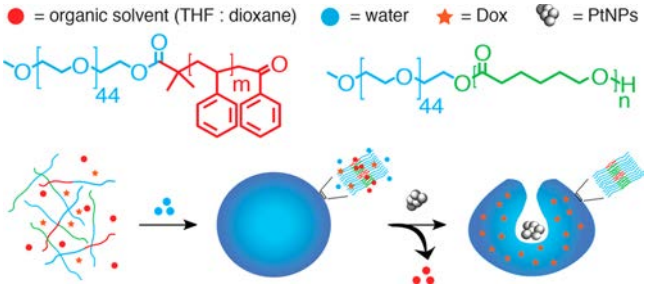

Figure 1. Self-assembly of a Dox-loaded hybrid stomatocyte nanomotor.

RESULTS AND DISCUSSION

Self-Assembly of Hybrid Polymersome or Stomatocyte. A hybrid polymersome or stomatocyte was prepared by mixing the biodegradable polymer PEG-*b*-PCL with the template polymer PEG-*b*-PS (0/100, 25/75, 50/50, 75/25, 90/10, and 100/0, w/w) by a solvent switch method and subsequent dialysis to induce osmotic shock and folding of the membrane into it.[56,57] Polymers with different ratios were dissolved in organic solvent (THF/dioxane = 4:1, v/v), and Milli-Q water was then slowly added into the polymer solution at a rate of 1 mL/h. After vigorous dialysis to remove the organic solvent, hybrid polymeric vesicles with different PCL percentages were obtained. No significant cloud point was observed in the sample with 100% PCL. This indicates no vesicle formation, which was also confirmed by dynamic light

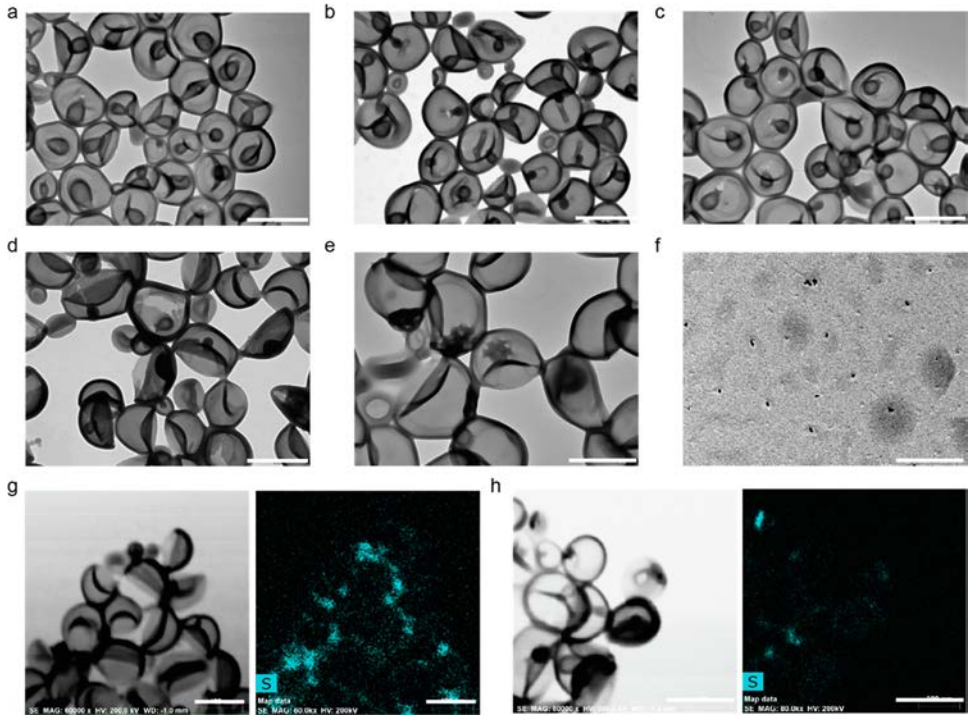

Figure 2. Characterization of vesicles with different percentages of PEG-*b*-PCL. (a) TEM measurements of vesicles with 0% PEG-*b*-PCL. (b) TEM measurements of vesicles with 25% PEG-*b*-PCL. (c) TEM measurements of vesicles with 50% PEG-*b*-PCL. (d) TEM measurements of vesicles with 75% PEG-*b*-PCL. (e) TEM measurements of vesicles with 90% PEG-*b*-PCL. (f) TEM measurements of samples with 100% PEG-*b*-PCL. (g) EDX of FITC-labeled vesicles with 50% PEG-*b*-PCL-FITC. (h) EDX of normal vesicles with 50% PEG-*b*-PCL. Scale bar is 500 nm.

DOI: 10.1021/acsnano.6b08079
ACS Nano 2017, 11, 1957–1963

scattering (DLS) measurements. Thirty nanometer sized nanoparticles were formed instead. All self-assembled structures showed narrow polydispersity (Supplementary Table 1) until the PCL percentage was increased up to 90%. In the 90% PCL sample, a small population of 30 nm sized nanoparticles was observed in DLS intensity data (Supplementary Figure 1), whereas the number size distribution DLS showed a much larger percentage of 30 nm nanoparticles (Supplementary Figure 2). This suggested high demixing between PEG-*b*-PS and PEG-*b*-PCL polymers and the assembly of the PEG-*b*-PCL into micelles. Transmission electron microscopy (TEM) was further used to visualize the morphology of these samples (Figure 2a–f). Vesicles containing PEG-*b*-PCL in less than 75% can form well-defined stomatocyte structures. Clear bilayer structure was observed with a thickness around 25 nm. Due to the bilayer structure, the hydrophilic drug Dox was loaded in the water lumen of vesicles during the self-assembly. Fluorescent Dox was observed in the confocal image as red dot indicating a successful drug encapsulation (Supplementary Figure 3).

Formation of PCL Domains. In order to confirm the mixing and the presence of PCL in the membrane structure, energy-dispersive X-ray spectroscopy (EDX) was used to map certain elements on the vesicles. Fluorescein isothiocyanate (FITC) was coupled onto the PEG-*b*-PCL polymer to introduce S for visualization. Significant S enrichment was observed for the FITC-labeled vesicles (mixed with 50% PEG-*b*-PCL-FITC) compared to normal vesicles without FITC labeling (mixed with 50% PEG-*b*-PCL) (Figure 2g,h). Interestingly, the signal of S showed domain formation on the structure of the hybrid vesicle rather than homogeneous distribution over the whole membrane. EDX line scans using STEM mode across the vesicles also revealed that S was not evenly distributed on the membrane structure (Supplementary Figure 4). Differential scanning calorimetry (DSC) was further used to confirm the demixing behavior of hybrid stomatocytes. The samples with different percentages of PCL blending (0, 25, 50, 75, 90, and 100% PCL) were prepared and freeze-dried for DSC measurements. From the DSC spectrum (Supplementary Figure 6), two polymers mixed well in the sample of the hybrid stomatocyte with 25% PCL blending due to a negligible signal from semicrystalline PCL. When the PCL percentage increased to 50%, a significant signal of PCL was observed, which suggests PCL demixing with PS, indicating PCL domain formation.

Because the main component of the hybrid stomatocytes (PEG-*b*-PCL polymer) is biodegradable, our nanomotor systems can easily be degraded by either acid or lipases. Stomatocytes with 50% PCL were used to investigate the acid-induced degradation as well-defined stomatocyte structures were still formed at this high percentage. Hybrid stomatocytes with 50% PCL were incubated with citric acid/Na_2HPO_4 buffer (pH 1), and scanning electron microscopy (SEM) was used to image the morphology changing before and after acidic treatment. From the SEM image and TEM image (inset of Figure 3a) shown in Figure 3a, smooth bowl-shaped stomatocytes with narrow openings were observed before treatment. However, after incubation with acidic buffer, the PCL units from the stomatocyte started to degrade (Figure 3b). Large pores in the membrane of the stomatocyte and even collapsed structures were formed. This also indicates that a high percentage of PEG-*b*-PCL polymer induces domain formation onto the membrane, which is responsible for the observation of

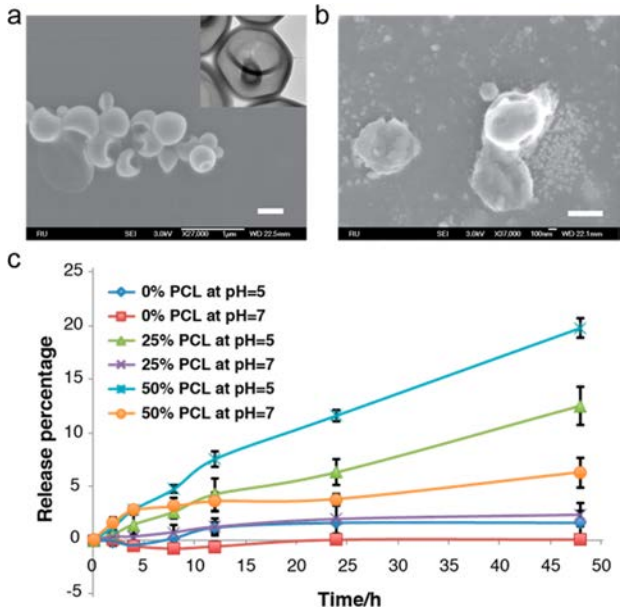

Figure 3. Pore formation of stomatocytes before and after degradation. (a) SEM images of stomatocytes with 50% PEG-*b*-PCL before acidic degradation (inset is a TEM image of a single stomatocyte with small opening). (b) SEM images of stomatocytes with 50% PEG-*b*-PCL after acidic degradation. (c) Release of Dox from a stomatocyte with different percentages of PCL at different pH. All scale bars are 400 nm.

the large pores by SEM after acid treatment. This would not be possible if PEG-*b*-PCL is homogeneously mixed with PEG-*b*-PS in the membrane.[58] When loaded with drug, the drug can be released in a controlled manner once PCL starts to degrade at low pH. This feature makes these motors attractive for practical drug delivery and release in the human body.

In order to investigate the release characteristics of our self-assembled system, release experiments *in vitro* from stomatocyte nanomotors were performed at room temperature in two types of medium, namely, acidic buffer (citric acid/Na_2HPO_4, pH 5) and neutral buffer (citric acid/Na_2HPO_4, pH 7) (Figure 3c). The release percentage of stomatocyte nanomotors with 50% PCL was higher than that of samples without PCL or with only 25% PCL in both acidic and neutral conditions. Moreover, for stomatocyte nanomotors without PCL blending, there was almost no release of Dox in both buffers at different pH. Hybrid nanomotors cumulatively release 20% Dox in acidic buffer for 48 h, which was significantly higher than the 5% release in buffer at pH 7 in the same time frame. Interestingly, the release curve of stomatocytes with 25% PCL and 50% PCL seemed to be quite linear, probably because of pore formation after acidic treatment. From SEM images after acidic incubation (Figure 3a,b), pores on the structure of the hybrid stomatocyte and collapsed structures were observed, which also explains the linear release profiles of Dox.

Movement Analysis and Cell Uptake. PEG-*b*-PS and PEG-*b*-PCL at different ratios were dissolved in THF and dioxane (4:1, v/v), and Milli-Q water was added at a rate of 1 mL/h followed by PtNP solution. After dialysis to remove the organic solvent, hybrid stomatocyte nanomotors with different PCL percentages were obtained (the structure of nanomotors can be seen in Supplementary Figure 7). Nanosight NS500 was used to investigate the motion behavior of these hybrid stomatocyte nanomotors in the presence of hydrogen peroxide

DOI: 10.1021/acsnano.6b08079
ACS Nano 2017, 11, 1957–1963

solution. The movement was recorded for 90 s, and each second contained 30 frames. Nanoparticle-tracking analysis was used to track in real-time the movement of the stomatocyte motors. A 4.98 mM hydrogen peroxide solution was used for the motion analysis. An appropriate concentration of motor solution (finally concentration is 10^8 particles/mL) was added, and the resulting solution was measured at physiological temperature of 37 °C. Calculated mean-square displacements (MSDs) of the hybrid nanomotors in the presence of hydrogen peroxide showed directional movement compared to that of the stomatocytes without fuel. Fitting of the MSDs allows for calculation of the velocity of the nanomotors by using the self-diffusiophoretic model proposed by Golestanian and co-workers.[59] The velocity of hybrid stomatocyte nanomotors in the presence of fuel (Figure 4a) at 37 °C showed no significant

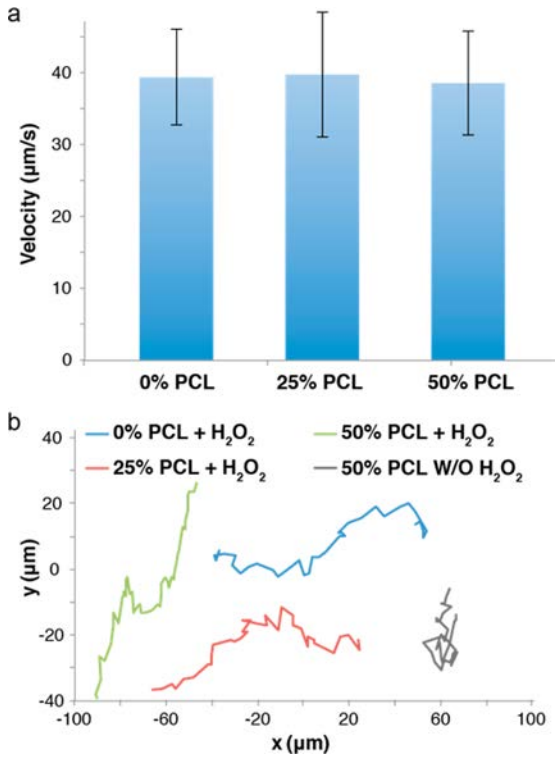

Figure 4. Motion of hybrid stomatocyte nanomotors with different percentage of PCL. (a) Velocity of hybrid stomatocyte nanomotors in the presence of H_2O_2 (final concentration was 4.98 mM) at 37 °C. The motion of the nanomotor was measured by Nanosight NS500. Velocities were calculated. Directional motion was fitted using the equation $(4D)\Delta t + (v^2)(\Delta t^2)$. (b) Representative tracking trajectories of the hybrid stomatocyte nanomotor.

difference compared to that of normal nanomotors without PCL blending, which was also comparable with our previous study. The velocity of the stomatocyte nanomotor with 0, 25, and 50% PCL was around 39 μm/s. Brownian motion and a typical linear MSD curve was observed when studying the movement of hybrid nanomotors without hydrogen peroxide fuel. In addition, representative tracking trajectories of the hybrid nanomotors with and without fuel are presented in Figure 4b. As predicted, the trajectory of the hybrid nanomotors without fuel followed the random walk typical of a Brownian motion and did not show any directionality or increase in movement. For the mechanism of motion, self-diffusiophoresis and bubble propulsion were possible mechanisms in our system. In our previous studies,[27] decreased speed and MSDs were observed in PBS compared to Milli-Q water, indicating a self-diffusiophoresis mechanism. However, speed and MSDs in PBS were still higher than those of motors without hydrogen peroxide fuel (Brownian motion), which also indicated the possible existence of a bubble propulsion mechanism. After degradation of the PCL in acidic conditions, the motion behavior of a biodegradable hybrid stomatocyte nanomotor was studied. Almost Brownian motion was observed, indicating that the degradation of PCL affects the motion behavior (Supplementary Figure 8). For our nanomotor design, the narrow opening of the stomatocyte serves as the outlet for the formed oxygen, and it is crucial for the propulsion of the nanomotor. After PCL degradation, large pores or even collapsed structures are formed on the membrane of the stomatocyte nanomotor. This results in complete collapse of the structure or of the outlet into multiple pores, leading to almost complete disruption of the active motion toward Brownian motion.

HeLa cells were used to investigate cell internalization and subsequent release behavior of hybrid stomatocyte nanomotors. The cells were incubated with Dox-loaded nanomotors together with hydrogen peroxide. Confocal laser scanning microscopy images (Figure 5) clearly show that both a normal stomatocyte nanomotor and a hybrid stomatocyte nanomotor were taken up by the HeLa cells (red fluorescence comes from Dox). In the case of a biodegradable hybrid stomatocyte nanomotor, the fluorescence of Dox diffused over the cell, indicating the release of drugs from vesicles into the cell due to degradation (see the cross section in Figure 5d). However, stomatocytes without PCL still showed a dot-like fluorescent signal (see the cross section in Figure 5b), which meant no drug release occurred. In addition, cell uptake experiments were also performed without hydrogen peroxide. Similar results are shown in Supplementary Figure 9. To further test the biodegradability of our nanomotor, stomatocytes loaded with near-infrared fluorescent cyanine dye DiR were injected *in vivo*. The fluorescence signal was no longer detectable at day 7 after injection, compared to the strong signal at day 3, suggesting that the stomatocytes were degraded in the mouse (Supplementary Figure 10).

CONCLUSIONS

In summary, we have demonstrated the design of a hybrid stomatocyte nanomotor based on biodegradable PCL for drug delivery. The bilayer membrane structure of motors allows for efficient loading of both hydrophilic and hydrophobic drugs. Due to a high percentage of PCL blending, PCL domains were formed on the surface of the nanomotors. The system is in effect able to locally sense the environment, in this case pH. During the degradation, pores and collapse are formed, leading to controlled release of the anticancer drug under acidic conditions *in vitro*. In addition, our nanomotor can also be taken up by HeLa cells and subsequently release its cargo to kill them. Finally, *in vivo* data show the biodegradability of the nanomotor system. Thus, we envision that our nanomotor system has huge potential for drug delivery and controlled released *in vivo*.

METHODS

Self-Assembly of Stomatocytes or Hybrid Stomatocytes. Ten milligrams of polymer with different ratios between PEG-*b*-PS and PEG-*b*-PCL was fully dissolved in a 1 mL mixture of THF/

DOI: 10.1021/acsnano.6b08079
ACS Nano 2017, 11, 1957–1963

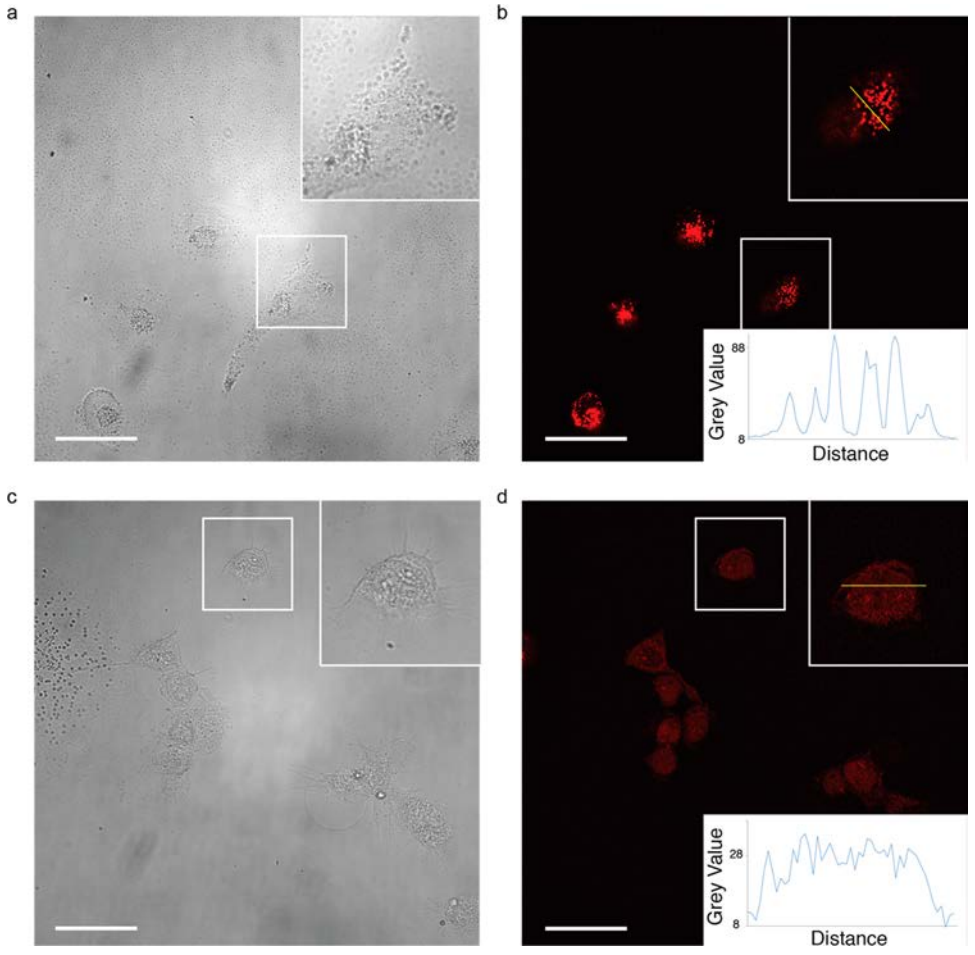

Figure 5. Cell uptake of Dox-loaded stomatocyte nanomotors. (a) Bright-field images of cells after being incubated with Dox-loaded stomatocyte nanomotors (without PEG-*b*-PCL) in hydrogen peroxide. (b) Confocal images of cells after exposure to Dox-loaded stomatocyte nanomotors without PEG-*b*-PCL. (c) Bright-field images of cells after being incubated with Dox-loaded stomatocyte nanomotors (50% PEG-*b*-PCL) in hydrogen peroxide. (d) Confocal images of cells after exposure to Dox-loaded stomatocyte nanomotors with 50% PEG-*b*-PCL. All scale bars are 20 μm.

dioxane (4:1, v/v). One milliliter of Milli-Q water was slowly added into the solution by a syringe pump at a rate of 1 mL/h. After vigorous dialysis for at least 48 h, stomatocytes and hybrid stomatocytes with different percentages of PCL were obtained.

Self-Assembly of PtNP-Loaded Stomatocyte or Hybrid PtNP-Loaded Stomatocyte. Ten milligrams of polymer with different ratios between PEG-*b*-PS and PEG-*b*-PCL was fully dissolved in a 1 mL mixture of THF/dioxane (4:1, v/v). Next, 0.35 mL of Milli-Q water was slowly added by a syringe pump at a rate of 1 mL/h, followed by addition of preformed PtNP solution (0.65 mL) also at a rate of 1 mL/h. After dialysis for at least 48 h, PtNP-loaded stomatocytes and hybrid PtNP-loaded stomatocytes with different percentages of PCL were obtained.

DSC Measurement of Hybrid Stomatocytes with Different Percentages of PCL. Hybrid stomatocyte samples with different percentages of PCL blending (0, 25, 50, 75, 90, and 100% PCL) were prepared by the solvent switch method. The samples were freeze-dried for DSC measurement. DSC thermograms were recorded using the Mettler DSC 822e (Mettler-Toledo AG, Greifensee, Switzerland). Samples (10 mg) were crimped in aluminum pans with pierced lids, equilibrated at 0 °C for 5 min, and finally heated to 100 °C at a heating rate of 2 °C/min. The measurement cell was purged with dry nitrogen gas at a flow rate of 50 mL/min during the measurements.

Movement Analysis. Nanosight NS500 was used for the motion measurements of hybrid stomatocyte nanomotors. Hydrogen peroxide solution (4.98 mM) was used for the motion analysis. Hybrid nanomotor solution with a final concentration around 10^8 particles/mL was added, and the resulting solution was measured at physiological temperature of 37 °C. The motion of hybrid stomatocyte nanomotors after acidic degradation was also measured. The fitting of the MSD allows for calculation of the speed of the nanomotors by using the self-diffusiophoretic model proposed by Golestanian and co-workers.[59] While a purely diffusive system would show only a linear component according to the equation $(4D)\Delta t$, from which an enhanced diffusion coefficient can be extracted, our MSD curves are not linear and show a parabolic fit according to the equation $(4D)\Delta t + (v^2)(\Delta t^2)$, from which we can extract the velocity of the particles.

ASSOCIATED CONTENT

Supporting Information

The Supporting Information is available free of charge on the ACS Publications website at DOI: 10.1021/acsnano.6b08079.

Supporting methods, figures, and tables (PDF)

AUTHOR INFORMATION

Corresponding Author

*E-mail: d.wilson@science.ru.nl.

ORCID

Daniela A. Wilson: 0000-0002-8796-2274

DOI: 10.1021/acsnano.6b08079
ACS Nano 2017, 11, 1957−1963

Author Contributions

Y.F.T and F.P. contributed equally. Y.F.T. and D.A.W. conceived and designed the experiments. Y.F.T., F.P., A.A.M.A., Y.J.M., and M.S. performed the experiments. Y.F.T. analyzed data and prepared the manuscript. All authors discussed the results and contributed to the final form of the manuscript.

Notes

The authors declare no competing financial interest.

ACKNOWLEDGMENTS

This work was financed by the European Research Council ERC-StG 307679 "StomaMotors". We acknowledge support from the Ministry of Education, Culture and Science (Gravitation program 024.001.035). D.A.W. acknowledges financial support from NWO Chemiche Wetenschappen VIDI Grant 723.015.001. M.S. acknowledges support from ERC-2014-StG-336454-CoNQUeST. F.P. acknowledges funding from the China scholarship council. Geert-Jan A. Janssen and the General Instruments department are acknowledged for providing support for the EDX measurements.

REFERENCES

(1) Wang, J. *Nanomachines: Fundamentals and Applications*; John Wiley & Sons: New York, 2013.
(2) Abdelmohsen, L. K.; Peng, F.; Tu, Y.; Wilson, D. A. Micro-and Nano-Motors for Biomedical Applications. *J. Mater. Chem. B* **2014**, *2*, 2395−2408.
(3) Sanchez, S.; Soler, L.; Katuri, J. Chemically Powered Micro- and Nanomotors. *Angew. Chem., Int. Ed.* **2015**, *54*, 1414−1444.
(4) Lin, X.; Wu, Z.; Wu, Y.; Xuan, M.; He, Q. Self-Propelled Micro-/Nanomotors Based on Controlled Assembled Architectures. *Adv. Mater.* **2016**, *28*, 1060−1072.
(5) Wang, W.; Duan, W.; Ahmed, S.; Sen, A.; Mallouk, T. E. From One to Many: Dynamic Assembly and Collective Behavior of Self-Propelled Colloidal Motors. *Acc. Chem. Res.* **2015**, *48*, 1938−1946.
(6) Wang, H.; Pumera, M. Fabrication of Micro/Nanoscale Motors. *Chem. Rev.* **2015**, *115*, 8704−8735.
(7) Wang, J.; Gao, W. Nano/Microscale Motors: Biomedical Opportunities and Challenges. *ACS Nano* **2012**, *6*, 5745−5751.
(8) Tu, Y.; Peng, F.; Adawy, A.; Men, Y.; Abdelmohsen, L. K.; Wilson, D. A. Mimicking the Cell: Bio-Inspired Functions of Supramolecular Assemblies. *Chem. Rev.* **2016**, *116*, 2023−2078.
(9) Palagi, S.; Mark, A. G.; Reigh, S. Y.; Melde, K.; Qiu, T.; Zeng, H.; Parmeggiani, C.; Martella, D.; Sanchez-Castillo, A.; Kapernaum, N.; et al. Structured Light Enables Biomimetic Swimming and Versatile Locomotion of Photoresponsive Soft Microrobots. *Nat. Mater.* **2016**, *15*, 647−653.
(10) Magdanz, V.; Stoychev, G.; Ionov, L.; Sanchez, S.; Schmidt, O. Stimuli-Responsive Microjets with Reconfigurable Shape. *Angew. Chem., Int. Ed.* **2014**, *53*, 2673−2677.
(11) Mei, Y.; Huang, G.; Solovev, A. A.; Ureña, E. B.; Mönch, I.; Ding, F.; Reindl, T.; Fu, R. K.; Chu, P. K.; Schmidt, O. G. Versatile Approach for Integrative and Functionalized Tubes by Strain Engineering of Nanomembranes on Polymers. *Adv. Mater.* **2008**, *20*, 4085−4090.
(12) Gao, W.; Sattayasamitsathit, S.; Orozco, J.; Wang, J. Highly Efficient Catalytic Microengines: Template Electrosynthesis of Polyaniline/Platinum Microtubes. *J. Am. Chem. Soc.* **2011**, *133*, 11862−11864.
(13) Zhang, L.; Petit, T.; Lu, Y.; Kratochvil, B. E.; Peyer, K. E.; Pei, R.; Lou, J.; Nelson, B. J. Controlled Propulsion and Cargo Transport of Rotating Nickel Nanowires near a Patterned Solid Surface. *ACS Nano* **2010**, *4*, 6228−6234.
(14) Gao, W.; Sattayasamitsathit, S.; Manesh, K. M.; Weihs, D.; Wang, J. Magnetically Powered Flexible Metal Nanowire Motors. *J. Am. Chem. Soc.* **2010**, *132*, 14403−14405.
(15) Zhang, L.; Abbott, J. J.; Dong, L.; Peyer, K. E.; Kratochvil, B. E.; Zhang, H.; Bergeles, C.; Nelson, B. J. Characterizing the Swimming Properties of Artificial Bacterial Flagella. *Nano Lett.* **2009**, *9*, 3663−3667.
(16) Maier, A. M.; Weig, C.; Oswald, P.; Frey, E.; Fischer, P.; Liedl, T. Magnetic Propulsion of Microswimmers with DNA-Based Flagellar Bundles. *Nano Lett.* **2016**, *16*, 906−910.
(17) Paxton, W. F.; Kistler, K. C.; Olmeda, C. C.; Sen, A.; St. Angelo, S. K.; Cao, Y.; Mallouk, T. E.; Lammert, P. E.; Crespi, V. H. Catalytic Nanomotors: Autonomous Movement of Striped Nanorods. *J. Am. Chem. Soc.* **2004**, *126*, 13424−13431.
(18) Ahmed, S.; Wang, W.; Bai, L.; Gentekos, D. T.; Hoyos, M.; Mallouk, T. E. Density and Shape Effects in the Acoustic Propulsion of Bimetallic Nanorod Motors. *ACS Nano* **2016**, *10*, 4763−4769.
(19) Wang, W.; Li, S.; Mair, L.; Ahmed, S.; Huang, T. J.; Mallouk, T. E. Acoustic Propulsion of Nanorod Motors Inside Living Cells. *Angew. Chem., Int. Ed.* **2014**, *53*, 3201−3204.
(20) Xuan, M.; Wu, Z.; Shao, J.; Dai, L.; Si, T.; He, Q. Near Infrared Light-Powered Janus Mesoporous Silica Nanoparticle Motors. *J. Am. Chem. Soc.* **2016**, *138*, 6492−6497.
(21) Ma, X.; Wang, X.; Hahn, K.; Sánchez, S. Motion Control of Urea-Powered Biocompatible Hollow Microcapsules. *ACS Nano* **2016**, *10*, 3597−3605.
(22) Pavlick, R. A.; Sengupta, S.; McFadden, T.; Zhang, H.; Sen, A. A Polymerization-Powered Motor. *Angew. Chem., Int. Ed.* **2011**, *50*, 9374−9377.
(23) Lee, T.-C.; Alarcón-Correa, M.; Miksch, C.; Hahn, K.; Gibbs, J. G.; Fischer, P. Self-Propelling Nanomotors in the Presence of Strong Brownian Forces. *Nano Lett.* **2014**, *14*, 2407−2412.
(24) Peng, F.; Tu, Y.; van Hest, J.; Wilson, D. A. Self-Guided Supramolecular Cargo-Loaded Nanomotors with Chemotactic Behavior towards Cells. *Angew. Chem.* **2015**, *127*, 11828−11831.
(25) Wilson, D. A.; Nolte, R. J.; Van Hest, J. C. Autonomous Movement of Platinum-Loaded Stomatocytes. *Nat. Chem.* **2012**, *4*, 268−274.
(26) Wu, Y.; Wu, Z.; Lin, X.; He, Q.; Li, J. Autonomous Movement of Controllable Assembled Janus Capsule Motors. *ACS Nano* **2012**, *6*, 10910−10916.
(27) Tu, Y.; Peng, F.; Sui, X.; Men, Y.; White, P. B.; van Hest, J. C.; Wilson, D. A. Self-Propelled Supramolecular Nanomotors with Temperature-Responsive Speed Regulation. *Nat. Chem.* **2016**, DOI: 10.1038/nchem.2674.
(28) Peng, F.; Tu, Y.; Men, Y.; van Hest, J.; Wilson, D. A. Supramolecular Adaptive Nanomotors with Magnetotaxis Behavior. *Adv. Mater.* **2017**, *29*, 1604996.
(29) Gao, W.; Wang, J. The Environmental Impact of Micro/Nanomachines: A Review. *ACS Nano* **2014**, *8*, 3170−3180.
(30) Wang, J. Self-Propelled Affinity Biosensors: Moving the Receptor around the Sample. *Biosens. Bioelectron.* **2016**, *76*, 234−242.
(31) Moo, J. G. S.; Pumera, M. Self-Propelled Micromotors Monitored by Particle-Electrode Impact Voltammetry. *ACS Sensors* **2016**, *1*, 949−957.
(32) Patra, D.; Sengupta, S.; Duan, W.; Zhang, H.; Pavlick, R.; Sen, A. Intelligent, Self-Powered, Drug Delivery Systems. *Nanoscale* **2013**, *5*, 1273−1283.
(33) Mou, F.; Chen, C.; Zhong, Q.; Yin, Y.; Ma, H.; Guan, J. Autonomous Motion and Temperature-Controlled Drug Delivery of Mg/Pt-Poly (N-isopropylacrylamide) Janus Micromotors Driven by Simulated Body Fluid and Blood Plasma. *ACS Appl. Mater. Interfaces* **2014**, *6*, 9897−9903.
(34) Gao, W.; Wang, J. Synthetic Micro/Nanomotors in Drug Delivery. *Nanoscale* **2014**, *6*, 10486−10494.
(35) Peng, F.; Tu, Y.; Adhikari, A.; Hintzen, J. C.; Löwik, D. W.; Wilson, D. A. A Peptide Functionalized Nanomotor as an Efficient Cell Penetrating Tool. *Chem. Commun.* **2017**, *53*, 1088−1091.

DOI: 10.1021/acsnano.6b08079
ACS Nano 2017, 11, 1957−1963

(36) Wu, Z.; Wu, Y.; He, W.; Lin, X.; Sun, J.; He, Q. Self-Propelled Polymer-Based Multilayer Nanorockets for Transportation and Drug Release. *Angew. Chem., Int. Ed.* **2013**, *52*, 7000−7003.
(37) Wu, Z.; Lin, X.; Si, T.; He, Q. Recent Progress on Bioinspired Self-Propelled Micro/Nanomotors via Controlled Molecular Self-Assembly. *Small* **2016**, *12*, 3080−3093.
(38) Soler, L.; Magdanz, V.; Fomin, V. M.; Sanchez, S.; Schmidt, O. G. Self-Propelled Micromotors for Cleaning Polluted Water. *ACS Nano* **2013**, *7*, 9611−9620.
(39) Ma, X.; Hahn, K.; Sanchez, S. Catalytic Mesoporous Janus Nanomotors for Active Cargo Delivery. *J. Am. Chem. Soc.* **2015**, *137*, 4976−4979.
(40) Schattling, P.; Thingholm, B.; Stadler, B. Enhanced Diffusion of Glucose-Fueled Janus Particles. *Chem. Mater.* **2015**, *27*, 7412−7418.
(41) Wu, Z.; Li, T.; Li, J.; Gao, W.; Xu, T.; Christianson, C.; Gao, W.; Galarnyk, M.; He, Q.; Zhang, L.; et al. Turning Erythrocytes into Functional Micromotors. *ACS Nano* **2014**, *8*, 12041−12048.
(42) Wu, Z.; Lin, X.; Zou, X.; Sun, J.; He, Q. Biodegradable Protein-Based Rockets for Drug Transportation and Light-Triggered Release. *ACS Appl. Mater. Interfaces* **2015**, *7*, 250−255.
(43) Gao, W.; Dong, R.; Thamphiwatana, S.; Li, J.; Gao, W.; Zhang, L.; Wang, J. Artificial Micromotors in the Mouse's Stomach: A Step toward in Vivo Use of Synthetic Motors. *ACS Nano* **2015**, *9*, 117−123.
(44) Li, J.; Thamphiwatana, S.; Liu, W.; Esteban-Fernández de Ávila, B.; Angsantikul, P.; Sandraz, E.; Wang, J.; Xu, T.; Soto, F.; Ramez, V.; et al. Enteric Micromotor Can Selectively Position and Spontaneously Propel in the Gastrointestinal Tract. *ACS Nano* **2016**, *10*, 9536−9542.
(45) Chen, C.; Karshalev, E.; Li, J.; Soto, F.; Castillo, R.; Campos, I.; Mou, F.; Guan, J.; Wang, J. Transient Micromotors That Disappear When No Longer Needed. *ACS Nano* **2016**, *10*, 10389−10396.
(46) King, J. C. Zinc: An Essential but Elusive Nutrient. *Am. J. Clin. Nutr.* **2011**, *94*, 679S−684S.
(47) Wacker, W. E.; Vallee, B. L. Magnesium Metabolism. *N. Engl. J. Med.* **1958**, *259*, 431−438.
(48) Klibanov, A. L.; Maruyama, K.; Torchilin, V. P.; Huang, L. Amphipathic Polyethyleneglycols Effectively Prolong the Circulation Time of Liposomes. *FEBS Lett.* **1990**, *268*, 235−237.
(49) Wilson, D. A.; de Nijs, B.; van Blaaderen, A.; Nolte, R. J.; van Hest, J. C. Fuel Concentration Dependent Movement of Supramolecular Catalytic Nanomotors. *Nanoscale* **2013**, *5*, 1315−1318.
(50) Abdelmohsen, L. K.; Nijemeisland, M.; Pawar, G. M.; Janssen, G.-J. A.; Nolte, R. J.; van Hest, J. C.; Wilson, D. A. Dynamic Loading and Unloading of Proteins in Polymeric Stomatocytes: Formation of an Enzyme-Loaded Supramolecular Nanomotor. *ACS Nano* **2016**, *10*, 2652−2660.
(51) Nijemeisland, M.; Abdelmohsen, L. K.; Huck, W. T.; Wilson, D. A.; van Hest, J. C. A Compartmentalized Out-of-Equilibrium Enzymatic Reaction Network for Sustained Autonomous Movement. *ACS Cent. Sci.* **2016**, *2*, 843−849.
(52) Chen, W.; Meng, F.; Cheng, R.; Zhong, Z. pH-Sensitive Degradable Polymersomes for Triggered Release of Anticancer Drugs: A Comparative Study with Micelles. *J. Controlled Release* **2010**, *142*, 40−46.
(53) Lu, Y.; Chen, S. Micro and Nano-Fabrication of Biodegradable Polymers for Drug Delivery. *Adv. Drug Delivery Rev.* **2004**, *56*, 1621−1633.
(54) Shuai, X.; Ai, H.; Nasongkla, N.; Kim, S.; Gao, J. Micellar Carriers Based on Block Copolymers of Poly (ε-caprolactone) and Poly (ethylene glycol) for Doxorubicin Delivery. *J. Controlled Release* **2004**, *98*, 415−426.
(55) Szatrowski, T. P.; Nathan, C. F. Production of Large Amounts of Hydrogen Peroxide by Human Tumor Cells. *Cancer Res.* **1991**, *51*, 794−798.
(56) Kim, K. T.; Zhu, J.; Meeuwissen, S. A.; Cornelissen, J. J.; Pochan, D. J.; Nolte, R. J.; van Hest, J. C. Polymersome Stomatocytes: Controlled Shape Transformation in Polymer Vesicles. *J. Am. Chem. Soc.* **2010**, *132*, 12522−12524.
(57) Meeuwissen, S. A.; Kim, K. T.; Chen, Y.; Pochan, D. J.; van Hest, J. Controlled Shape Transformation of Polymersome Stomatocytes. *Angew. Chem., Int. Ed.* **2011**, *50*, 7070−7073.
(58) LoPresti, C.; Massignani, M.; Fernyhough, C.; Blanazs, A.; Ryan, A. J.; Madsen, J.; Warren, N. J.; Armes, S. P.; Lewis, A. L.; Chirasatitsin, S.; et al. Controlling Polymersome Surface Topology at the Nanoscale by Membrane Confined Polymer/Polymer Phase Separation. *ACS Nano* **2011**, *5*, 1775−1784.
(59) Howse, J. R.; Jones, R. A.; Ryan, A. J.; Gough, T.; Vafabakhsh, R.; Golestanian, R. Self-Motile Colloidal Particles: From Directed Propulsion to Random Walk. *Phys. Rev. Lett.* **2007**, *99*, 048102.

DOI: 10.1021/acsnano.6b08079
ACS Nano 2017, 11, 1957−1963